Kilohertz *in vivo* imaging of neural activity

*Jianglai Wu[1, 2, 3], Yajie Liang[3], Ching-Lung Hsu[3], Mariya Chavarha[4], Stephen W Evans[4], Donqging Shi[4], Michael Z Lin[4], Kevin K Tsia[2, *], and Na Ji[1, 3, 5*]*

[1]Department of Physics, Department of Molecular and Cell Biology, Helen Wills Neuroscience Institute, University of California, Berkeley, CA, USA

[2]Department of Electrical and Electronic Engineering, The University of Hong Kong, Pokfulam Road, Hong Kong, China

[3]Janelia Research Campus, Howard Hughes Medical Institute, Ashburn, VA, USA

[4]Department of Bioengineering, Stanford University, Stanford, California, USA

[5]Molecular Biophysics and Integrated Bioimaging Division, Lawrence Berkeley National Laboratory, Berkeley, CA, USA

*To whom correspondence should be addressed: tsia@hku.hk, jina@berkeley.edu

Understanding information processing in the brain requires us to monitor neural activity *in vivo* at high spatiotemporal resolution. Using an ultrafast two-photon fluorescence microscope (2PFM) empowered by all-optical laser scanning, we imaged neural activity *in vivo* at 1,000 frames per second and submicron spatial resolution. This ultrafast imaging method enabled monitoring of electrical activity down to 300 μm below the brain surface in head fixed awake mice.

The ability to monitor neural signaling at synaptic and cellular resolution *in vivo* holds the key to dissecting the complex mechanisms of neural activity in intact brains of behaving animals. The past decade has witnessed a proliferation of genetically encoded fluorescence indicators that monitor diverse neural signaling events *in vivo*, including those sensing calcium transients, neurotransmitter and neuromodulator release, and membrane voltage [1]. Most popular are the calcium indicators (e.g., GCaMP6 [2]) and glutamate sensors (e.g., iGluSnFR [3]), with their success partly attributable to their slow temporal dynamics (e.g., rise and decay times of 100 – 1000's milliseconds for GCaMP6 and tens of milliseconds for iGluSnFR), which can be adequately sampled with conventional 2PFM systems. Indeed, using point scanning and near-infrared wavelength for fluorescence excitation, 2PFM can routinely image calcium activity hundreds of microns deep in opaque brains with submicron spatial resolution [4-6].

Imaging faster events, however, is more challenging. Indicators reporting membrane voltage, arguably the most direct and important measure of neural activity, have rise and decay

times measured in milliseconds. Too fast for the frame rate of conventional 2PFM to match, their *in vivo* imaging demonstrations were mostly carried out by widefield fluorescence microscopy with comparatively poor spatial resolution and limited to superficial depths of the brain [7, 8]. In other words, the capability of state-of-the-art indicators has outstripped our ability to image them at sufficiently high speed, especially at high spatial resolution and in large depths of scattering brains.

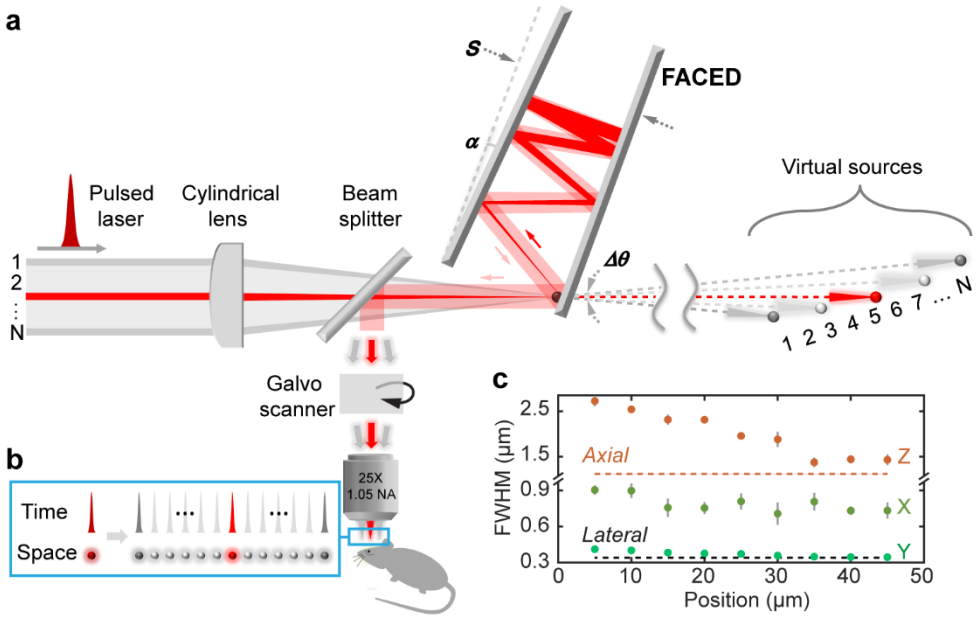

Figure 1: Principles and resolution of a 2PFM with a FACED module. (a) Schematic of a FACED microscope. A 1-MHz collimated femtosecond laser was focused into a nearly parallel mirror pair with a converging angle $\Delta\theta$ by a cylindrical lens. After multiple reflections, the misalignment angle α caused the beamlets to retroreflect (e.g., the red rays). Beamlets at different incidence angles (e.g., red versus gray rays) emerged with distinct propagation directions and temporal delays. Equivalently, the sequence of multiple beamlets ($N = \Delta\theta/\alpha$) at the output of the FACED module can be treated as light emanating from an array of virtual sources. These beamlets were then coupled into a 2PFM, and formed (b) an array of spatially separated and temporally delayed foci at the focal plane of a microscope objective. (c) The focal spot sizes along the X/FACED, Y, and Z axes, measured from 200-nm-diameter fluorescent beads. Error bars show s.d. from 10 beads; dashed lines indicate the expected axial and lateral resolutions at 1.05 NA.

The imaging speed of conventional 2PFM is limited by laser scanners, such as galvanometric mirrors, to tens of frame per second (fps) [5, 6]. Its effective pixel dwell time (typically microseconds) is much longer than the ultimate limit imposed by the fluorescence lifetime (typically nanoseconds), below which substantial crosstalk of fluorescence from neighboring pixels can occur [9]. By leveraging an all-optical, passive laser scanner based on a concept termed free-space angular-chirp-enhanced delay (FACED) [10], here we demonstrated 2PFM at 1,000 fps, with the pixel dwell time flexibly configured to reach the fluorescence lifetime. We applied it to ultrafast monitoring of calcium activity, glutamate release, and action potentials

with a variety of activity indicators. We showed that this ultrafast 2PFM can image both spontaneous and sensory-evoked action potentials in awake mouse brains *in vivo*.

The principle of FACED was detailed previously (**Fig. 1a**) [10]. Briefly, a pulsed laser beam was focused in 1D by a cylindrical lens and obtained a converging angle $\Delta\theta$. It was then launched into a pair of almost parallel high-reflectivity mirrors with separation S and misalignment angle α. After multiple reflections by the mirrors, the laser beam/pulse was split into multiple beamlets/subpulses ($N = \Delta\theta/\alpha$) of distinct propagation directions and eventually retroreflected with an inter-pulse temporal delay of $2S/c$, with c being the speed of light. After being relayed to enter a microscope objective, this pulse train formed an array of spatially separated and temporally delayed foci (**Fig. 1b**). In a fluorescent sample, they excited two-photon fluorescence in succession, which could be detected by a photomultiplier tube, sampled at high speed, and assigned to individual foci and image pixels. Effectively, this passive FACED module allows line scanning at the repetition rate of the pulsed laser, typically MHz.

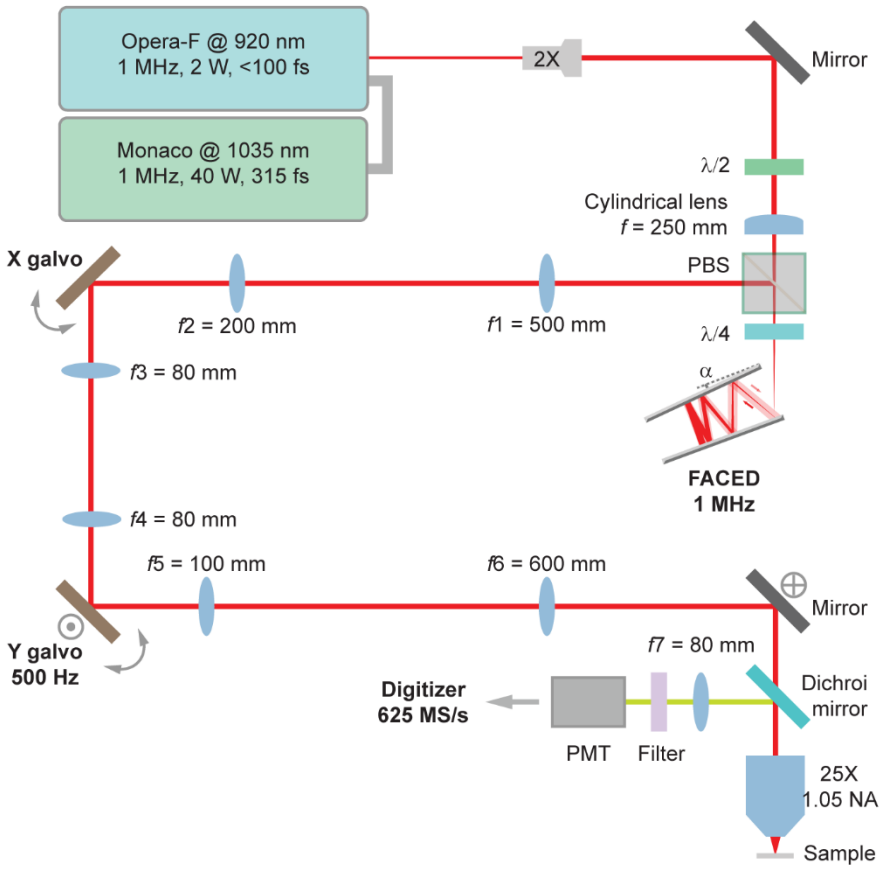

Supplementary Figure 1: Optical layout of the FACED two-photon fluorescence microscope. 2X: 2-fold beam expander; λ/2: Half-wave plate; PBS: polarizing beam splitter; λ/4: quarter-wave plate; α: misalignment angle of the mirror pair; PMT: photomultiplier tube. The FACED module scans the foci along the X galvo direction. Note that the X galvo is deactivated for high-speed functional imaging.

In this work, we designed a FACED module to incorporate into a standard 2PFM upgraded with a high-speed data acquisition system (625 MS/s) (**Supplementary Methods**, **Supplementary Fig. 1**). With a laser system of 1 MHz repetition rate, our FACED module

scanned 80 pulsed foci spanning 50 μm at 1 MHz. The inter-pulse interval was chosen to be 2 ns to reduce pixel crosstalk due to fluorescence lifetime and detector response time. We measured the full width at half maxima (FWHMs) of these foci by imaging 200-nm-diameter fluorescent beads. From the first to last, the foci were images of virtual sources formed after distinct numbers of mirror reflections and located at increasing distances away (**Fig. 1a**), with the more distant virtual sources leading to larger beam sizes at the back focal plane of the objective. As a result, the more temporally delayed pulses have smaller foci along both the lateral and axial directions (**Fig. 1c**). The beams filled the back focal plane more along the Y than X/FACED axis, and gave rise to ~0.8 μm (X) and ~0.35 μm (Y) lateral resolution, sufficient to resolve subcellular structures. With the FACED module providing 1 MHz line scan rate, we obtained a frame rate of 1,000 fps by scanning the Y galvanometer at 500 Hz and collecting data bidirectionally. The additional X galvanometer allowed us to tile the images to cover a larger field of view, if desired.

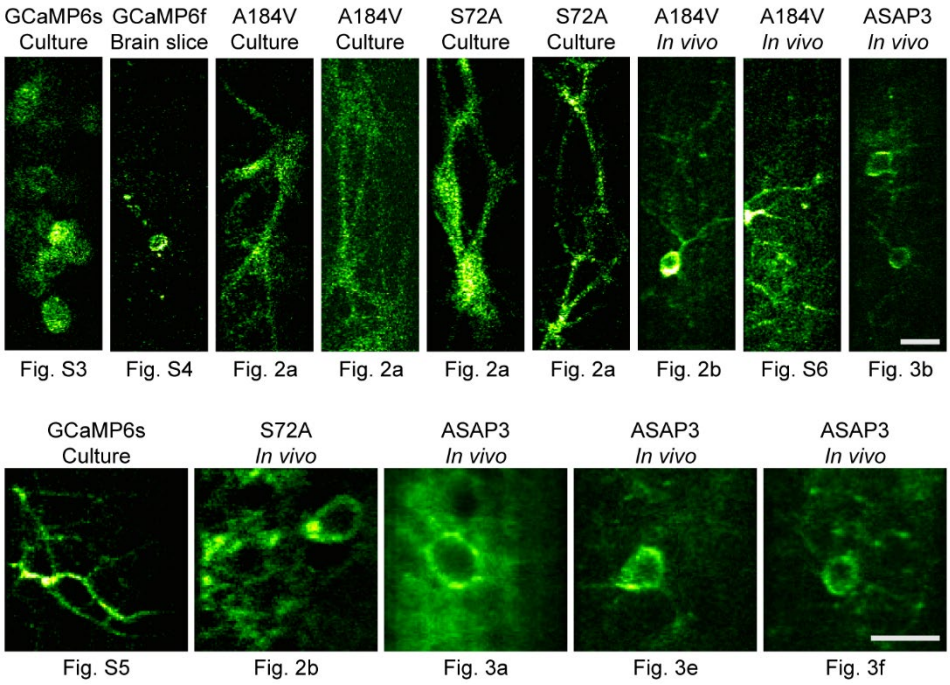

Supplementary Figure 2: Representative raw images taken at 1000 fps for different indicators presented in this work. Calcium indicators: GCaMP6s and GCaMP6f; Glutamate indicators: A184V and S72A variants of iGluSnFR; voltage indicator: ASAP3. Scale bars are 20 μm.

We first used the FACED 2PFM to image calcium dynamics using genetically encoded calcium indicators GCaMP6s and 6f [2]. At 1 kHz, morphological features were clearly resolved in individual images (see **Supplementary Fig. 2** for representative raw images taken at 1 kHz for all data presented in this manuscript). We reliably detected calcium transients in GCaMP6s cultured neurons (**Supplementary Fig. 3** and **Video 1**) and GCaMP6f acute mouse brain slices (**Supplementary Fig. 4** and **Video 2**) that were evoked by extracellular electric stimulation. Due to its high spatiotemporal resolution, we could clearly resolve neurites in cultured neurons, and in

one case, we recorded spontaneous calcium releases in neurites which then propagated at 25 μm/s across the dendrites (**supplementary Fig. 5** and **video 3**).

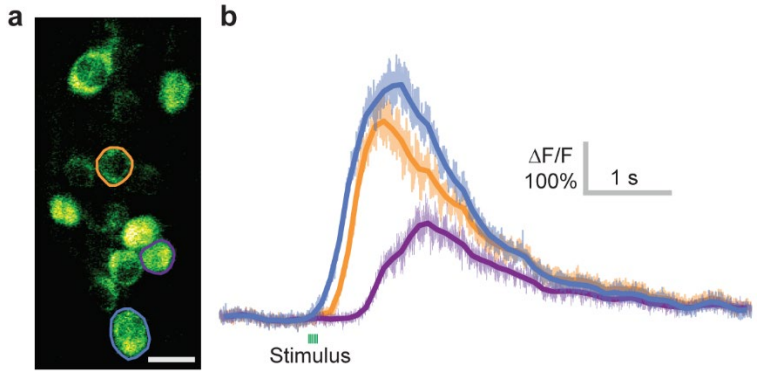

Supplementary Figure 3: 1 kHz imaging of GCaMP6s-expressing cultured neurons. (a) Morphological image. (b) Calcium transients of 3 cells in (a) evoked by field electrode stimulation and recorded at 1,000 fps. Darker lines were 100-point boxcar averages of the raw traces to guide the eye. Scale bar: 20 μm.

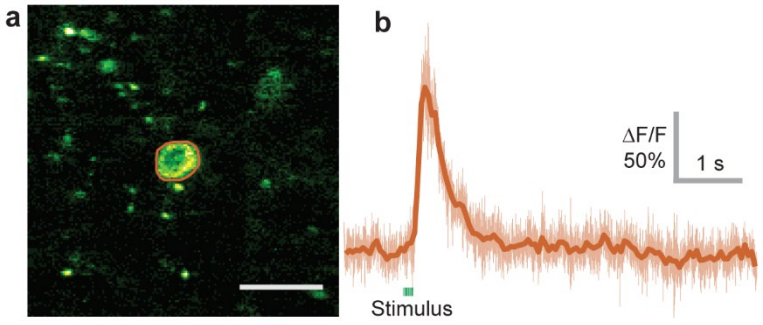

Supplementary Figure 4: 1 kHz imaging of a GCaMP6f-expressing neuron in an acute brain slice. (a) Morphological image. (b) Calcium transient of the cell in (a) evoked by field electrode stimulation and recorded at 1,000 fps. Darker line was 50-point boxcar average of the raw trace to guide the eye. Scale bar: 20 μm.

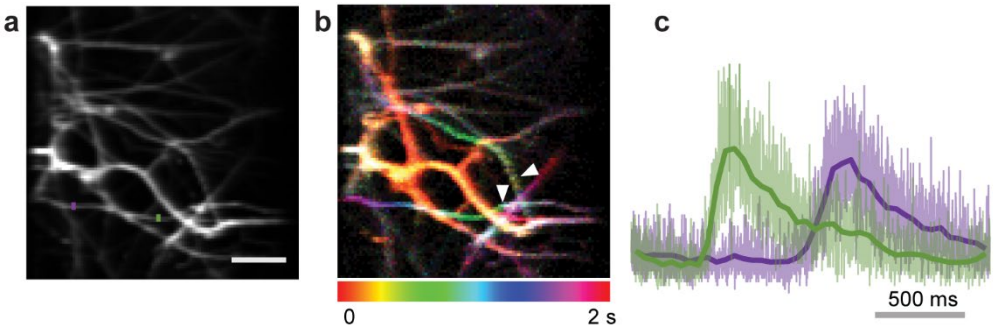

Supplementary Figure 5: 1 kHz imaging of spontaneous calcium increases in neurites of GCaMP6s-expressing cultured neurons. (a) Mean intensity projection of 2,000 frames. (b) Temporal color coding of the 2,000 frames highlights the sites where calcium increases were initially observed (white arrowheads). (c) Calcium transients at the color masked positions in (a), indicating a calcium propagating speed of ~25 μm/s. Darker lines were 50-point boxcar averages of the raw traces to guide the eye. Scale bar: 10 μm.

Clearly, the true power of FACED lies in imaging faster physiological events. Next, we imaged neurons labeled with variants A184V and S72A of the genetically encoded glutamate sensor iGluSnFR, which were expressed at cell membranes and had faster kinetics than the calcium indicators [11]. FACED 2PFM reliably reported glutamate release events evoked by field stimulation in cultured neurons (**Fig. 2a** and **Supplementary videos 4-7**), as well as spontaneous

glutamate release in L2/3 neurons in the primary visual cortex (V1) of head-fixed awake mice (**Fig.2b** and **Supplementary videos 8-9**). Both in culture and *in vivo*, we observed faster

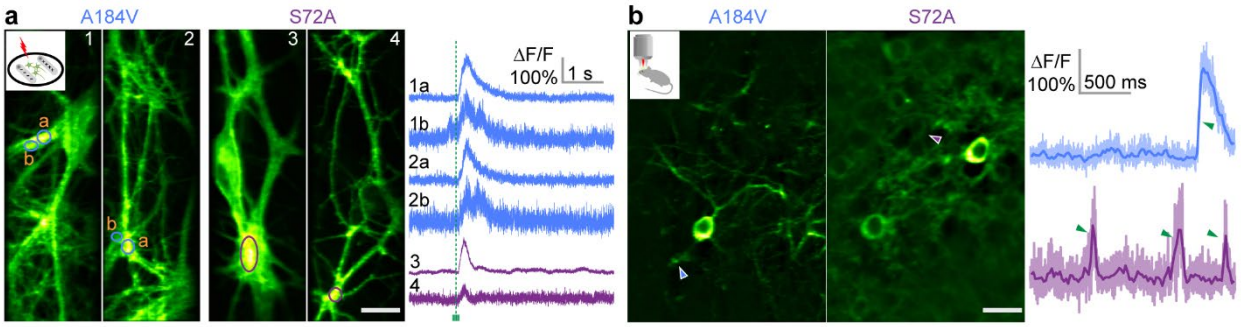

Figure 2: 1 kHz imaging of genetically encoded glutamate indicator iGluSnFR variants in cultured neurons and in V1 of awake mice *in vivo*. (a) (Left) mean intensity projections of cultured neurons expressing either the A184V or the S72A variants of iGluSnFR; (Right) transients associated with glutamate release triggered by extracellular electric stimulation (green dashed line) for structures labeled on the left. (b) (Left) Representative images of layer 2/3 neurons (depth: 150 – 250 μm) expressing either A184V or S72A in V1 of awake mice; (Right) Transients associated with spontaneous glutamate releases at sites indicated by arrowheads on the left. Here, darker lines were 20-point boxcar averages of the raw traces to guide the eye. Green arrowheads on the traces highlight the fast rising edge of the glutamate transients. Scale bars: 20 μm. "Green hot" lookup table in ImageJ was applied to all images. Post-objective power: 25 – 30 mW for cultured neurons, 40 mW *in vivo*.

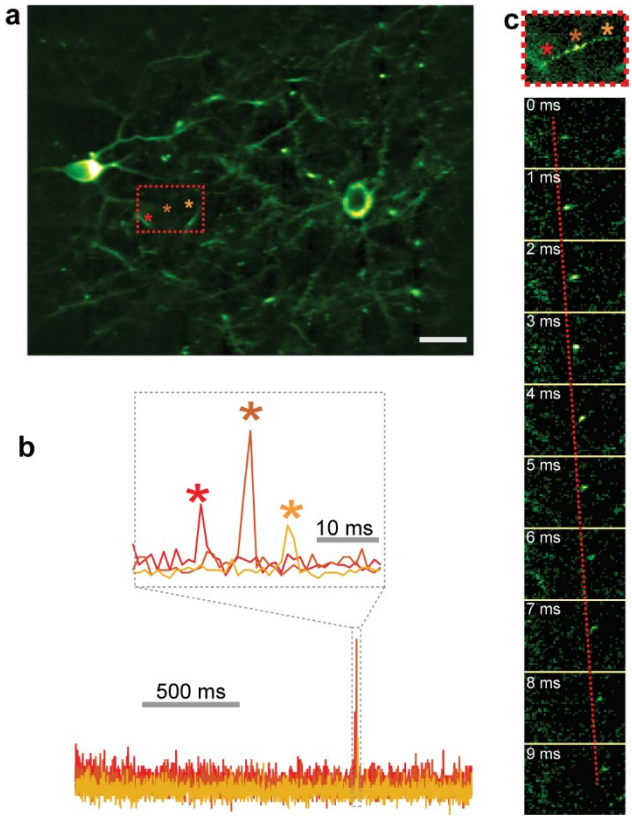

Supplementary Figure 6: Tracking rapid movement of a fluorescent particle in the awake mouse brain *in vivo*. (a) Morphological image of layer 2/3 neurons expressing the A184V variant of the glutamate sensor iGluSnFR in V1 of an awake mouse. (b) Time traces at the three pixels indicated by the three asterisks in (a). (c) Top panel shows the maximum intensity projection of the 10 image frames collected at 1 kHz of the boxed region in (a); bottom panel shows the 10 individual frames imaged at 1 ms interval. Scale bars: 20 μm.

dynamics from the lower-affinity variant S72A than A184V, consistent with the sensor characterizations by conventional 2PFM [11]. Imaging the brain *in vivo* at 1,000 fps, we also observed rapid movements of fluorescent particles, which transited the field of view at ~1 mm/s (**Supplementary Fig. 6** and **Supplementary video 10**). We speculated that they were macrophages containing fluorescent remnants of dead cells and moving rapidly with blood flow in the vasculature. The ability of FACED 2PFM to capture such rapid event indicates that this method can also be used to study rapid biological events associated with blood flow.

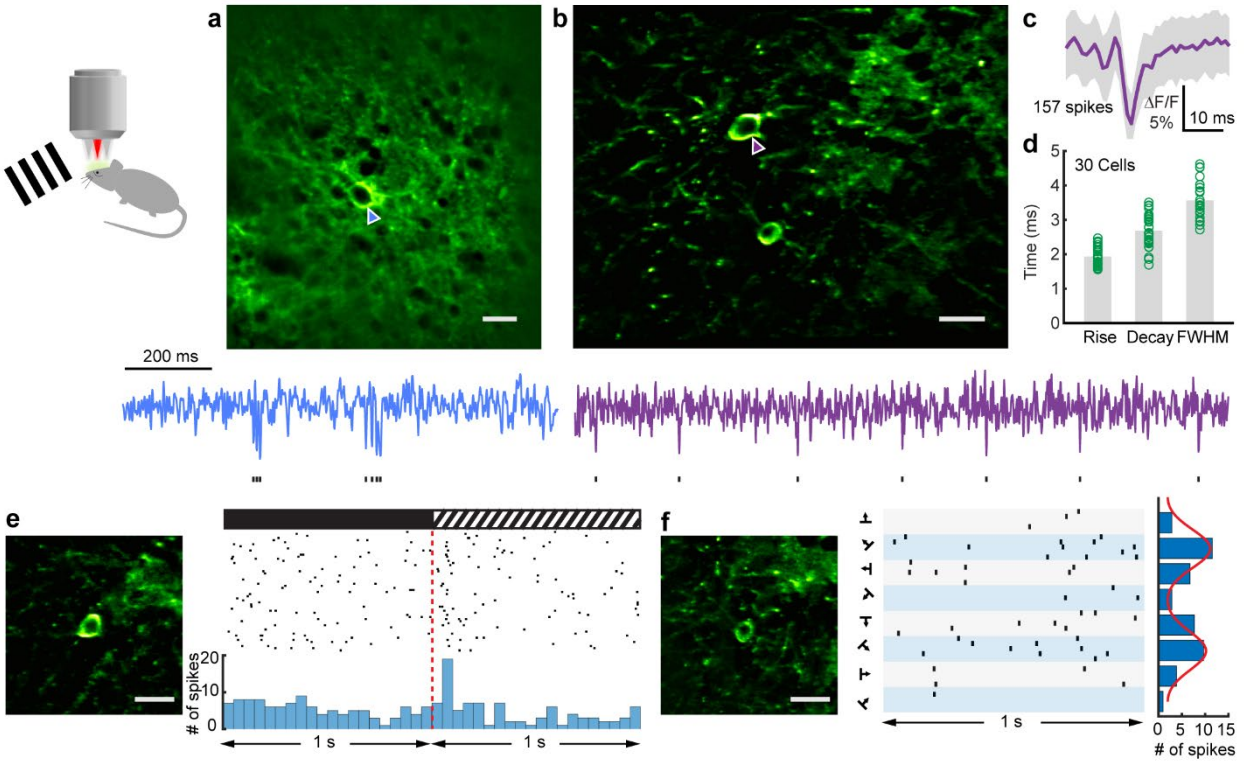

Figure 3: 1 kHz imaging of voltage responses in V1 of awake mice. (a, b) (Top) Representative images of L2/3 neurons in V1 either (a) densely or (b) sparsely labeled with ASAP3, a genetically encoded voltage indicators; (Bottom) Representative traces from neurons in (a) and (b), indicated by blue and purple arrow heads, respectively. Short black ticks below the traces denote optical spikes identified as downward deflections beyond three standard deviations (s.d.) of the trace. (c) Average of 157 optical spikes detected within 160 s from the neuron in (b); gray shaded area: s.d. (d) The rise time, decay time, and FWHM of the optical spikes measured from 30 neurons. (e) A L2/3 V1 neuron exhibiting both spontaneous (in the dark) and visually evoked (by drifting grating stimuli) voltage activity. (Left) morphology of the neuron; (Right, upper panel) raster plot of optical spikes over 80 trials (trials without detected spikes are not plotted); (Right, lower panel) histogram of spike counts within 50-ms bins. Dashed red line: stimulus onset. (f) A V1 neuron with orientation selectivity. (Left) morphology of the neuron; (Middle) raster plots showing all the optical spikes detected from the neuron during the presentation of gratings drifting in 8 different directions with 5 trials each; (Right) Histogram of total optical spikes for each grating stimulus, with a double Gaussian fit (red line). All imaged neurons were at a depth of 250 – 300 μm below the brain surface. Scale bars: 20 μm. "Green hot" lookup table in ImageJ was used for all images. Post-objective power: 50 mW.

Finally and most importantly, we imaged neurons expressing genetically encoded voltage indicator ASAP3 [12] in V1 of head-fixed awake mice. Among all voltage indicators, the ASAP family are currently the only ones that monitor voltage signal in brain slice or *in vivo* with 2PFM, albeit within very restricted field of views [12-14]. As an inverse sensor, ASAP3 reports membrane depolarizations and action potentials as downward deflections in fluorescence. The FACED microscope allowed us to detect spontaneous voltage signals corresponding to putative action potentials in both densely and sparsely labeled V1 neurons at depth down to 250 – 300 μm below the brain surface (**Figs. 3a**, **b**).

We observed substantial signal decrease within the first 1 s of imaging (**Supplementary Fig. 7**). However, ASAP3 fluorescence recovered almost completely in images collected seconds later (**Supplementary Fig. 8**), allowing us to interrogate voltage responses from the same structures repeatedly. Despite photobleaching, downward signals corresponding to individual action potentials ("optical spikes") could be easily detected in single trials with SNR > 3 (see **Methods**, **Supplementary Fig. 9**, **Figs. 3a, b**). In one neuron, we detected 157 action potentials within 160 s of recording (**Fig. 3c**). From the average fluorescence waveform of this (**Fig. 3c**) and 29 other neurons (**Supplementary Fig. 10**), the rise time, decay time, and FWHM of ASAP3 signal corresponding to single action potential were determined to be 1.93 ± 0.28 ms, 2.68 ± 0.48 ms, and 3.57 ± 0.51 ms, respectively (**Fig. 3d**). These characteristic time constants are consistent with those measured in an independent work [12].

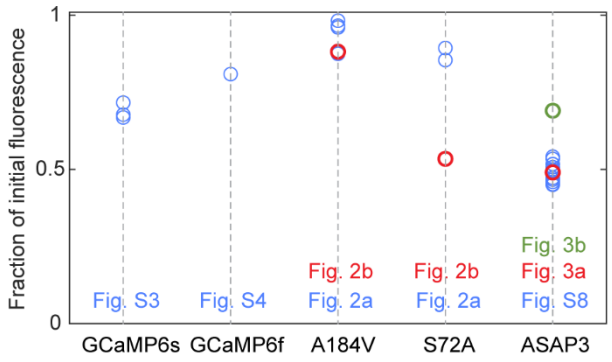

Supplementary Figure 7: Fluorescence bleaching for all the raw traces. Vertical axis indicates the ratio between the mean fluorescence signal of the last 50 frames and first 50 frames for a sequence of 1,000 frames imaged at 1,000 fps.

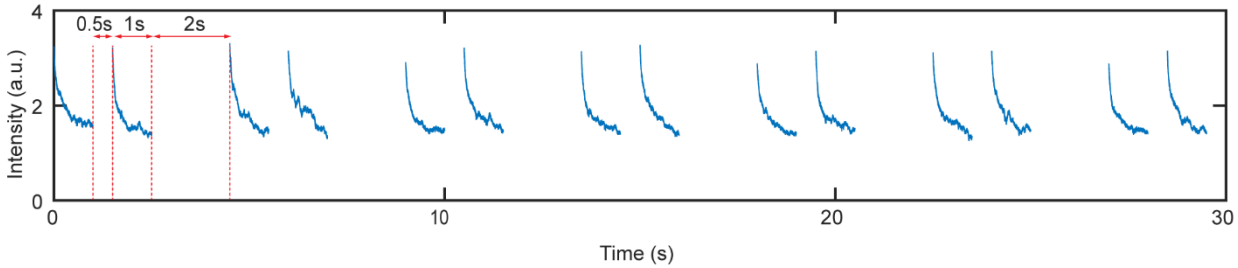

Supplementary Figure 8: 14 raw fluorescence traces recorded within 30 seconds from the same cell in Fig. 3a. Each trace was obtained from 1,000 frames recorded at 1,000 fps.

FACED 2PFM could also detect visually evoked spiking responses of neurons in V1 of awake mice. In one example (**Fig. 3e**), we detected action potentials from a V1 neuron, with the mouse being presented with a dark screen interleaved with drifting grating stimuli. This neuron was active both in the dark and during grating presentation, as was typical for V1 neurons measured electrophysiologically with cell-attached recording. Also consistent with electrophysiological recordings, there was an increase in firing rate following the onset of visual stimuli and with a latency of 50 – 100 ms, reflecting the beginning of grating-evoked activity in V1 [15, 16]. We also recorded a neuron with orientation selectivity, and found a 5.5× higher firing rate for the preferred orientation than the null orientation, corresponding to an orientation selectivity index of 0.7 (**Fig. 3f**).

In summary, using an all-optical passive laser scanner based on FACED, we achieved ultrafast kilohertz imaging of neural activity with subcellular resolution in the mouse brain *in vivo*. The highest average power used in these experiments, 50 mW post objective, remains within the safe range and substantially below the threshold for heating-induced damages [17]. We did not observe signs of photodamages (e.g., blabbing of dendrites) in any of the samples tested, suggesting higher-order nonlinear photodamage processes to be also minimal. This is expected, because the power of individual beamlet post objective was less than 0.6 mW and overlaying tissue further reduced the actual focal energy as a result of scattering loss. Furthermore, subsequent excitation pulses arrived at the same sample positions after 1 μs delay, providing ample time for the fluorophores to return from their photodamage-prone dark states back to their ground electronic state, a process that was shown to reduce photobleaching and increase fluorophore brightness [18].

Pushing the speed of two-photon fluorescence imaging to its fundamental limit, i.e. with a pixel dwell time similar to fluorescence lifetime, the FACED approach is readily compatible with conventional galvanometer-based 2PFMs and transform them to achieve kHz frame-rate imaging. Moreover, it follows conventional raster scanning strategy, requires minimal computational processing, and thus is immune to noise crosstalk effects observed in computation-based high-speed imaging techniques using, for example, compress sensing [19] or frequency multiplexing [20]. With existing sensors, FACED 2PFM have enough speed and sensitivity to detect calcium and glutamate transients from neuronal processes, and spiking events from cell bodies. Future improvement in brightness and sensitivity of voltage indicators should allow voltage signal to be

146 detected from subcellular compartments, which should allow FACED imaging to fulfill its full
147 potential in interrogating the electrical activity in the brain *in vivo* at synaptic resolution.

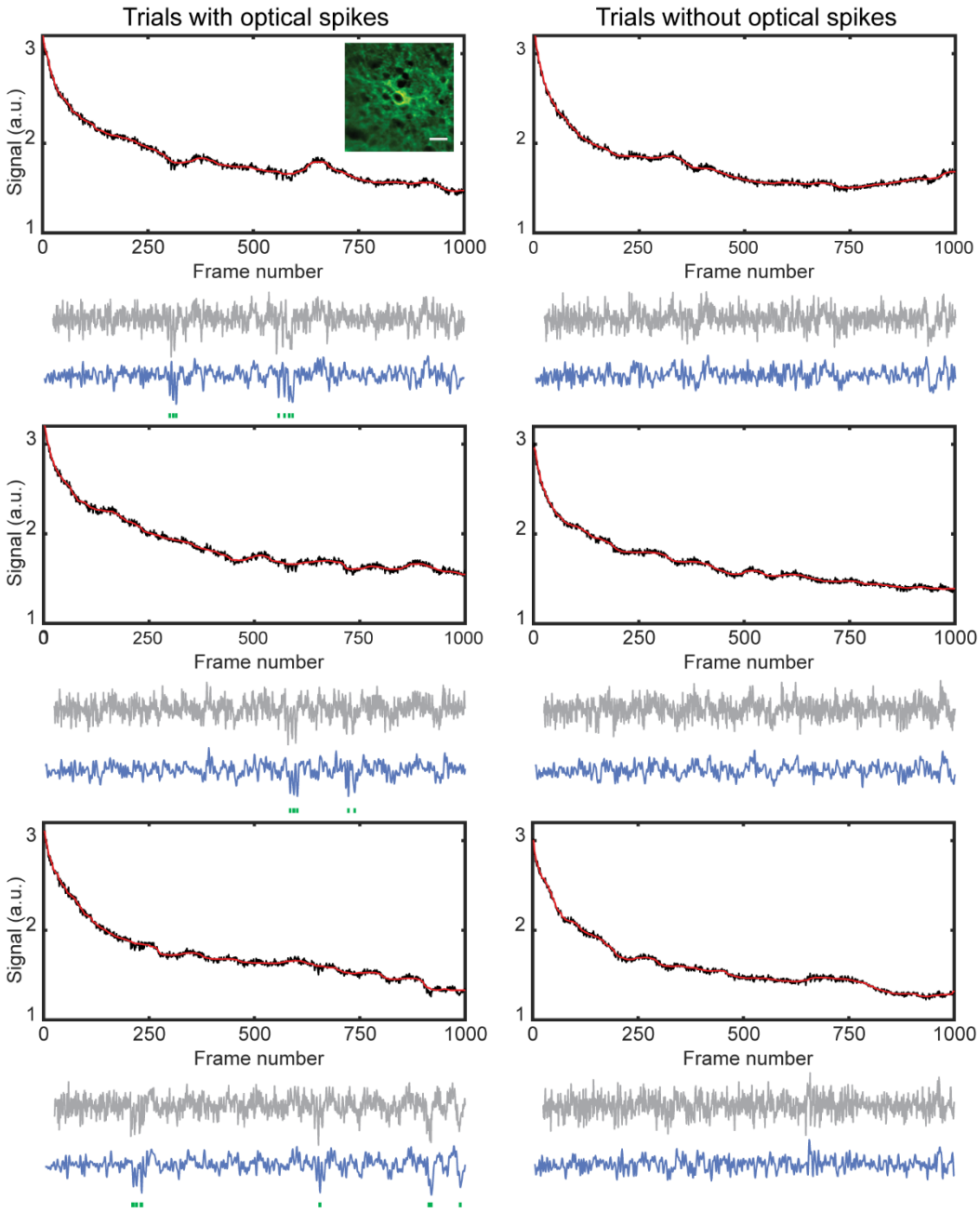

Supplementary Figure 9: Data processing for *in vivo* voltage traces. Left and right columns show three representative one-second voltage traces from the same neuron (as in Fig. 3a) with and without optical spikes detected, respectively. Inset: neuron image; scale bar: 20 μm. (Top) Baseline fluorescence F (red) was obtained by low pass filtering (50 ms median filter) of the raw traces (black); (Middle) $\Delta F/\sqrt{F}$ traces (fluorescence change to noise ratio, gray) was calculated and (bottom) subjected to a 200 Hz low pass Butterworth filter (blue). As ASAP3 is an inverse indicator, we define as optical spikes (green ticks) all downward deflections beyond three standard deviations of the trace.

Supplementary Figure 10: Voltage traces from 30 neurons. Purple curves are the averaged voltage trace (ΔF/F) corresponding to an action potential from individual neurons. Gray shaded area: s.d. of the raw traces. The rise time, decay time, and FWHM of the averaged optical spike as well as total number of detected spikes are listed for each neuron.

METHODS

Animals

All animal experiments were conducted according to the National Institutes of Health guidelines for animal research. Procedures and protocols on mice were approved by the Institutional Animal Care and Use Committee at Janelia Research Campus, Howard Hughes Medical Institute.

FACED two-photon fluorescence microscope (2PFM)

The simplified schematic of the FACED 2PFM is shown in **Supplementary Fig. 1a**. The two-photon excitation laser source at 920 nm (1 MHz repetition rate, 2 W maximal average output power, < 100 fs pulse width) was generated by an optical parametric amplifier (Opera-F, Coherent Inc.) that was pumped by a fiber laser (Monaco 1035-40-40, Coherent Inc.). After dispersion compensation [21], the laser beam was expanded with a 2× beam expander (BE02M-B, Thorlabs). A cylindrical lens (LJ1267RM-B, Thorlabs) then one-dimensionally focused the beam into a nearly parallel mirror pair (reflectivity > 99.9% at 920 nm, fused silica substrate, 250 mm long and 20 mm wide) with a separation of 300 mm. Because of the misalignment angle α, all the light rays eventually reflected back, following a set of zig-zig paths determined by their angles of incidence. After the FACED module, the rays (e.g. red rays in **Fig. 1a**) subjected to the same number of reflections by the mirror pair formed a single beamlet, and can be considered as emanating from a virtual light source located far away from the mirror pair. In this work, the retroreflected light rays formed 80 beamlets, and had their propagation distances within the FACED module (or their distance from their respective virtual sources) monotonically increase from ~10 m to ~60 m. The power throughput of the FACED module was ~40%.

A polarization beam splitter (CCM1-PBS253, Thorlabs) in combination with a half-wave plate (AHWP05M-980, Thorlabs) and quarter-wave plate (AQWP05M-980, Thorlabs) were used to direct the spatially and temporally separated pulse trains into a 2PFM. A pair of singlet lenses (LA1380-B-ML and LA4102-B-ML, Thorlabs) was used to conjugate the focal plan of the cylindrical lens and the X galvo (6215H, Cambridge Technology); a pair of achromat doublets (AC508-080-B and AC508-080-B,Thorlabs) was then used to conjugate the X galvo to the Y galvo (6215H, Cambridge Technology); another pair of singlet lenses (014-0990 and 014-1310, OptoSigma) were used to conjugate the Y galvo to the back focal plane of a 25×/1.05 NA water-dipping objective lens (XLPLN25XWMP2, Olympus) that was mounted on a piezo stage (P-725K094, Physik Instrumente). By tuning the misalignment angle between the two mirrors, we generated a sequence of 80 focal spots extending 50 μm along the X axis. With the separation between the two mirrors set at 300 mm, the time delay between adjacent pulses was 2 ns.

The two-photon excited fluorescence signal was collected by the same microscope objective, reflected by a dichroic mirror (FF665-Di02-25×36, Semrock), focused by a singlet lens (AC508-080-A, Thorlabs), and after passing through an emission filter (FF01-680/SP, Semrock), detected by a photomultiplier tube (PMT, H7422-40, Hamamatsu). The PMT signal was sampled

at 625 MS/s with a high speed digitizer and the data was transferred to and saved by a desktop computer through a PCIe 16× interface.

With 1 MHz repetition rate of the laser, the FACED module gave rise to a line scan rate of 1 MHz. Using the Y galvo to scan the foci along the direction orthogonal to the X/FACED axis at 500 Hz, and collecting the data bidirectionally, we achieved a frame rate of 1,000 fps with an effective image size of 80 × 900 pixels. 80 was given by the number of foci in the FACED axis and 900 was the product of the effective frame time (1 ms frame time minus a 100 μs dead time during mirror turns) and line scan rate. To increase the number of pixels in the FACED/X axis, X galvo was stepped to tile FACED images and increase the field of view. In this work, all functional imaging data were captured at 1,000 fps. For morphological imaging, we scanned the Y galvo at 50 Hz, resulting in a FACED imaging frame rate of 100 fps. (**Supplementary Table 1** listed all the major imaging parameters used in this work).

Supplementary Table 1: Major imaging parameters used in this work.

Specimen	**Cultured neurons**				**Brain slice**	**Awake mice in vivo**				
Figure number	Fig. 2a		Fig. S3	Fig. S5	Fig. S4	Fig. 2b & Fig. S6		Fig. 3a	Fig. 3b	Fig. 3e-3f
Indicator	A184V	S72A	GCaMP6s		GCaMP6f	A184V	S72A	ASAP3		
	High speed functional imaging									
FACED frame time (ms)	1									
FOV along x-axis (μm)	50									
FOV along y-axis (μm)	150			50	150	50			150	50
	Morphological imaging									
FACED frame time (ms)	N/A		10	N/A	10					
# of frames averaged	N/A		1	N/A	1	5				
FOV along x-axis (μm)	N/A		50	N/A	50					
FOV along y-axis (μm)	N/A		150	N/A	150			200	150	
Imaging depth (μm)	N/A					150 ~ 250		250 ~ 300		
Laser power (mW)	25	30	20		40			50		

The raw data from the digitizer was saved as 1D waveforms. The Gen-1 PCIe 16× slot on the data acquisition computer had a maximal streaming rate of 250 Mb/s, which caused the data to overflow the on-chip memory of the digitizer after 6 s of data acquisition and thus limited the data collection to up to 6-s bouts. Upgrading the computer with Gen-3 PCIe 16× interface should allow us to stream data continuously. At 1 kHz frame rate, each image frame had 625 × 900 sampling points, with 100 × 900 data points sampling actual fluorescence excitation by the FACED foci and used to reconstruct a single image. If desired, multi-line scans were averaged to generate a single X line in the final image: for a Y-axis range of 150 μm, 3 line scans were

averaged to form a single row; for a Y-axis range of 50 μm, 9 line scans are averaged. The final images were motion-registered with an iterative cross-correlation-based registration algorithm [22]. For morphological imaging, each FACED image frame had 625 × 9000 sampling points (10× exposure time), and a 10× increase in line averaging to form the final image.

Analysis of activity data

We manually selected regions of interests (ROIs) from the averaged images of the registered image sequence. The mean fluorescent intensity within the ROIs was used to calculate the ΔF/F time traces, with F being the baseline fluorescence and ΔF being the fluorescence change due to neural activity. In the calcium and glutamate indicator datasets, to calculate the ΔF/F, we calculated the baseline fluorescence F by fitting the data points away from the transients (e.g. the first and last 1000 data points in Fig. 2a) with a single exponential function.

In the voltage indicator datasets, the ROI was selected to efficiently cover the cell membrane and a 45 – 55 ms median filter was applied to the raw trace to get the fluorescence baseline F. The calculated ΔF (functional change) time trace is normalized to √F (Poisson noise) [23] and further subjected to a 200-Hz 8th order low-pass Butterworth filter. From the resulted traces, downward deflections beyond a threshold of 3σ (σ is the standard deviation of the trace) was classified as an "optical spike" corresponding to a putative action potential (**Supplementary Fig. 9**). To quantify the temporal dynamics of the optical voltage response, we aligned the optical spikes from the same neuron at peak response, and measured the rise (10% to 90%), decay (90% to 10%) and FWHM time from their averaged traces.

For the neuron whose response exhibited orientation selectivity (**Fig. 3f**), we fit its spike responses with a bimodal Gaussian function [22],

$$R(\theta) = R_{offset} + R_{pref} e^{-\frac{ang(\theta-\theta_{pref})^2}{2\sigma^2}} + R_{oppo} e^{-\frac{ang(\theta-\theta_{pref}+180)^2}{2\sigma^2}},$$

in which R_{offset} is the offset, θ_{pref} is the preferred grating drifting angle, R_{pref} and R_{oppo} are the responses at θ_{pref} and θ_{pref}-180 degree, respectively. The function $ang(x)$ = min (|x|, |x − 360|, |x + 360|) wraps angular values onto the interval 0° to 180°. The orientation selectivity index was calculated as the ratio between $R_{pref} - R_{ortho}$ and $R_{pref} + R_{ortho}$ where R_{ortho} is the response of the neuron to the orientation orthogonal to the preferred orientation.

Preparation and electric stimulation of primary neuronal culture

Primary neuronal cultures from neonatal rat pups were prepared as described previously [24]. AAV2/1.syn.GCaMP6s (1.8×10^{13} GC/ml), AAV.DJ.syn.iGluSnFR.A184V (3×10^{12} GC/ml), and AAV.DJ.syn.iGluSnFR.S72A (8.0×10^{12} GC/ml) were used to label cultured neurons by adding 1 μl of viral solution to each well in 24 well plates with 300 μl medium inside, respectively. After incubation overnight, 1 ml culture medium was added to each well. Neurons were imaged between 10 – 21 days post-transfection at room temperature in imaging buffer (145 mM NaCl, 2.5 mM KCl, 10 mM glucose, 10 mM HEPES, 2 mM $CaCl_2$, 1 mM $MgCl_2$, pH7.4).

For electric stimulation, cultured neurons in imaging buffer were positioned between two parallel electrodes separated at ~10 mm. A stimulus isolator (NPIISO-01D100, ALA Scientific Instruments Inc.) and functional generator (AFG1022, Tektronix Inc.) was used to generate the electric field. For each stimulation, a train of 10 pulses (pulse duration: 1 ms; period: 12 ms; voltage: 50 V) was used to drive the neurons.

Preparation and electric stimulation of acute brain slices

25-week-old male transgenic mice expressing GCaMP6f (scnn1a-TG3-cre x Ai93 x ACTB-tTA) [25, 26] were decapitated under deep isoflurane anesthesia, and the brain was transferred to an ice-cold dissection solution containing (in mM): 204.5 sucrose, 2.5 KCl, 1.25 NaH_2PO_4, 28 $NaHCO_3$, 7 dextrose, 3 Na-pyruvate, 1 Na-ascorbate, 0.5 $CaCl_2$, 7 $MgCl_2$ (pH 7.4, oxygenated with 95% CO_2 and 5% O_2). 350-μm-thick coronal slices of the primary visual cortex (V1) were sectioned using a vibrating tissue slicer (Leica VT 1200S, Leica Microsystems, Wetzlar, Germany). The slices were then transferred to a suspended mesh within an incubation chamber filled with artificial cerebrospinal fluid (ACSF) containing (in mM): 125 NaCl, 2.5 KCl, 1.25 NaH_2PO_4, 25 $NaHCO_3$, 25 dextrose, 1.3 $CaCl_2$, 1 $MgCl_2$ (pH 7.4, oxygenated with 95% CO_2 and 5% O_2). After 30 – 60 minutes of recovery at 35°C, the chamber was maintained at room temperature.

During imaging, slices were submerged in a recording chamber constantly perfused with oxygenated ACSF. A micropipette filled with ACSF were used for monopolar stimulation via a stimulus isolator (NPIISO-01D100, ALA Scientific Instruments Inc.) and a function generator (AFG1022, Tektronix Inc.). To provide extracellular stimulation, the stimulating electrode was placed in the proximity of the recorded cell, and a train of 10 pulses (pulse duration: 1 ms; period: 12 ms; current: 300 μA) was applied.

Mouse preparation for *in vivo* imaging

Mice (females or males, >2-months-old) were housed in cages (in groups of 1 – 5 before surgeries and in pairs or single housed after) under reverse light cycle. Wild-type (Jackson Laboratories, Black 6, stock #:000664) as well as Gad2-IRES-cre (Jackson Laboratories, Gad2tm2 (cre) Zjh/J, stock #: 010802) mice were used.

Virus injection and cranial window implantation procedures have been described previously [22]. Briefly, mice were anaesthetized with isoflurane (1 – 2% by volume in O_2) and given the analgesic buprenorphine (SC, 0.3 mg per kg of body weight). Animals were head fixed in a stereotaxic apparatus (Model 1900, David Kopf Instruments). A 3.5-mm diameter craniotomy was made over the left V1 with dura left intact. A glass pipette (Drummond Scientific Company) beveled at 45° with a 15 – 20 μm opening was back-filled with mineral oil. A fitted plunger controlled by a hydraulic manipulator (Narishige, MO10) was inserted into the pipette and used to load and slowly inject 30 nl viral solution into the brain (~200 – 400 μm below pia). 3 – 6 injection sites were chosen in the left V1 with 0.3 to 0.5 mm space between injection sites. The following viral vectors were used to label neurons with different sensors. Dense labeling with glutamate sensors: AAV.DJ.syn.iGluSnFR.A184V (3×10^{12} GC/ml); AAV.DJ.syn.iGluSnFR.S72A (8.0×10^{12} GC/ml); sparse labeling with glutamate sensors: AAV.DJ.syn.FLEX.iGluSnFR.A184V (2.8×10^{13} GC/ml) 1:1 mixed with AAV2/1.syn.Cre (500 times diluted from 1.5×10^{13} GC/ml); AAV.DJ.syn.FLEX.iGluSnFR.S72A (5.2×10^{12} GC/ml) 1:1 mixed with AAV2/1.syn.Cre (500 times diluted from 1.5×10^{13} GC/ml); dense labeling with the voltage sensor: AAV2/9.syn.ASAP3 (1.5×10^{12} GC/ml); sparse labeling with the voltage sensor: AAV2/9.CAG.FLEX.ASAP3 (6.7×10^{12} GC/ml) 1:1 mixed with AAV2/1.syn.Cre (500 times diluted from 1.5×10^{13} GC/ml). At the completion of viral injections, a glass window made of a single coverslip (Fisher Scientific No. 1.5) was embedded in the craniotomy and sealed in place with dental acrylic. A titanium head-post was then attached to the skull with cyanoacrylate glue and dental acrylic. *In vivo* imaging was carried out after at least two weeks of recovery with single or paired housing and habituation for head fixation. All imaging experiments were carried out on head-fixed awake mice.

Visual stimulation in head-fixed awake mice

Visual stimuli were presented by a liquid crystal display (7-inch diagonal and 1920 × 1200 pixels). The screen was positioned at 15 cm from the eye of the mice and orientated at ~40° to the long axis of the mice. Drifting sinusoidal gratings were presented for 1.5 s at 8 orientations (0° to 315° at 45° steps) in pseudorandom sequences. Between the grating stimulus, 3s dark screen were presented. Gratings had 100% contrast and 0.06 cycle per degree and drifted at 1.5 Hz. During

each 1.5 s stimulation period, a sequence of 1,000 images were recorded from 0 s to 1 s; during each 3 s dark adaptation period, a sequence of 1,000 images were recorded from 1.5 s to 2.5 s. A total of 5 or 10 trials were repeated for each stimulus.

Data processing

Unless stated otherwise, all images and data presented here were unprocessed raw images/data, without smoothing, denoising, or deconvolution. All data in the Supplementary Videos were collected at 1,000 fps, but were binned every 20 or 50 frames (no binning in **Supplementary Video 10**) and saved at 20 binned fps for video output by Fiji [27], which was not capable of saving videos at 1,000 fps. “Green hot” lookup table in ImageJ was used for all images.

ACKNOWLEDGEMENTS

The authors thank Cristina Rodriguez for help with the laser system; Rongwen Lu for help with visual stimulation experiments; Guan Cao for providing cultured neuron samples; Jonathan Marvin, Loren Looger for providing glutamate sensors; and the Janelia JET team for designing and assembling the dispersion compensation unit. This work was supported by Howard Hughes Medical Institute (J.W., Y.L., C.-L.H., N.J.), and American Epilepsy Society predoctoral fellowship (M.C.); the China Scholarship Council Joint PhD Training Program (D.S.); Stanford Neuroscience PhD Program training grant 5T32MH020016 and the Post-9/11 GI Bill (S.W.E.); Research Grants Council of the Hong Kong Special Administrative Region of China (17209017, 17259316, 17207715) (J.W., K.K.T.); and NIH BRAIN Initiative grants 1U01NS103464 (M.Z.L.), 1RF1MH114105 (M.Z.L.), and 1UF1NS107696 (J.W., N.J.).

CONTRIBUTIONS

NJ conceived of the project; ML, KKT, and NJ supervised research; JW, KKT, and NJ designed FACED module; JW, YL, CLH collected calcium imaging data; JW and YL collected glutamate sensing data; MC created ASAP3; MC, SE, and DS characterized ASAP3 and ASAP3-expressing viruses; JW and YL collected voltage sensing data; JW analyzed data; JW and NJ wrote the manuscript with inputs from all authors.

CONFLICT OF INTERESTS

The authors declare the following competing interests: KKT and The University of Hong Kong have filed a U.S. patent application (14/733,454) that relates to the all-optical laser-scanning imaging methods.

SUPPLEMENTARY VIDEO INFORAMTION

Supplementary video 1: Imaging calcium transients at 1,000 fps in GCaMP6s-expressing cultured neurons evoked by extracellular electric stimulation. Same data as in Supp. Fig. 3. The raw image sequence was binned every 50 frames, saved at 20 binned fps, and compressed for video output.

Supplementary video 2: Imaging calcium transients at 1,000 fps in GCaMP6f-expressing neurons in acute mouse brain slices evoked by extracellular electric stimulation. Same data as in Supp. Fig. 4. The raw image sequence was binned every 50 frames, saved at 20 binned fps, and compressed for video output.

Supplementary video 3: Imaging spontaneous calcium release events at 1,000 fps in neurites of GCaMP6s-expressing cultured neurons. Same data as in Supp. Fig. 5. The raw image sequence was binned every 20 frames, saved at 20 binned fps, and compressed for video output.

Supplementary videos 4-5: Imaging glutamate transients at 1,000 fps in cultured neurons expressing A184V variant of iGluSnFR evoked by extracellular electric stimulation. Same A184V data as in Fig. 2a. The raw image sequence was binned every 50 frames, saved at 20 binned fps, and compressed for video output.

Supplementary videos 6-7: Imaging glutamate transients at 1,000 fps in cultured neurons expressing S72A variant of iGluSnFR evoked by extracellular electric stimulation. Same S72A data as in Fig. 2a. The raw image sequence was binned every 50 frames, saved at 20 binned fps, and compressed for video output.

Supplementary video 8: Imaging glutamate transients of layer 2/3 neurons expressing A184V variant of iGluSnFR in V1 of awake mice at 1,000 fps. The white arrow points to the glutamate releasing site. Same A184V data as in Fig. 2b. The raw image sequence was binned every 20 frames, saved at 20 binned fps, and compressed for video output.

Supplementary video 9: Imaging glutamate transients of layer 2/3 neurons expressing S72A variant of iGluSnFR in V1 of awake mice at 1,000 fps. The white arrow points to the glutamate releasing site. Same S72A data as in Fig. 2b. The raw image sequence was binned every 20 frames, saved at 20 binned fps, and compressed for video output.

Supplementary video 10: Imaging rapid movement of a fluorescent particle at 1,000 fps in the layer 2/3 of awake mouse brain *in vivo*. Same data as in Supp. Fig. 6. A sequence of 50 raw images recorded at 1,000 fps was saved at 20 fps and compressed for video output.

REFERENCES:

1. Lin M.Z. & Schnitzer M.J. Genetically encoded indicators of neuronal activity. Nat. Neurosci.**19**, 1142–1153 (2016). DOI: https://doi.org/10.1038/nn.4359
2. Chen, T., et al. Ultrasensitive fluorescent proteins for imaging neuronal activity. Nature **499**, 295–300 (2013). DOI: https://doi.org/10.1038/nature12354
3. Marvin J.S., et al. An optimized fluorescent probe for visualizing glutamate neurotransmission. Nature Methods **10**, 162–170 (2013). DOI: https://doi.org/10.1038/nmeth.2333
4. Helmchen F. & Denk W. Deep tissue two-photon microscopy. Nat. Methods **2**, 932–940 (2005). DOI: https://doi.org/10.1038/nmeth818
5. Ji, N., Freeman, J. & Smith, S.L. Technologies for imaging neural activity in large volumes. Nat. Neurosci. **19**, 1154–1164 (2016). DOI: https://doi.org/10.1038/nn.4358
6. Yang, W. & Yuste, R. *In vivo* imaging of neural activity. Nat. Methods **14**, 349–359 (2017). DOI: https://doi.org/10.1038/nmeth.4230
7. Cao, G., et al. Genetically targeted optical electrophysiology in intact neural circuits. Cell **154**, 904–913 (2013). DOI: https://doi.org/10.1016/j.cell.2013.07.027
8. Gong, Y., et al. High-speed recording of neural spikes in awake mice and flies with a fluorescent voltage sensor. Science **350**, 1361–1366 (2015). DOI: https://doi.org/10.1126/science.aab0810
9. Chan, A.C.S., et al. Speed-dependent resolution analysis of ultrafast laser-scanning fluorescence microscopy. J. Opt. Soc. Am. B **31**, 755–764 (2014). DOI: https://doi.org/10.1364/JOSAB.31.000755
10. Wu, J.L., et al. Ultrafast laser-scanning time-stretch imaging at visible wavelengths. Light Sci. Appl. **6**, e16196 (2016). DOI: https://doi.org/10.1038/lsa.2016.196
11. Marvin, J.S., et al. Stability, affinity and chromatic variants of the glutamate sensor iGluSnFR. Nat. Methods **15**, 936–939 (2018). DOI: https://doi.org/10.1038/s41592-018-0171-3
12. Chavarha, M., et al. Fast two-photon volumetric imaging of an improved voltage indicator reveals electrical activity in deeply located neurons in the awake brain. Preprint at https://www.biorxiv.org/content/early/2018/10/17/445064 (2018).
13. Yang, H. H., et al. Subcellular imaging of voltage and calcium signals reveals neural processing *in vivo*. Cell **166**, 245–257 (2016).

DOI: https://doi.org/10.1016/j.cell.2016.05.031

14. Chamberland, S., et al. Fast two-photon imaging of subcellular voltage dynamics in neuronal tissue with genetically encoded indicators. eLife **6**, e25690 (2017). DOI: https://doi.org/10.7554/eLife.25690
15. Resulaj, A., Ruediger, S., Olsen, S.R. & Scanziani, M. First spikes in visual cortex enable perceptual discrimination. eLife **7**, e34044 (2018). DOI: https://doi.org/10.7554/eLife.34044
16. Ma, W. p., et al. Visual representations by cortical somatostatin inhibitory neurons—selective but with weak and delayed responses. J. Neurosci. **30**, 14371–14379 (2010). DOI: https://doi.org/10.1523/JNEUROSCI.3248-10.2010
17. Podgorski, K. & Ranganathan, G. Brain heating induced by near-infrared lasers during multiphoton microscopy. J. Neurophysiol. **116**, 1012–1023 (2016). DOI: https://doi.org/10.1152/jn.00275.2016
18. Donnert, G., Eggeling, C. & Hell, S. W. Major signal increase in fluorescence microscopy through dark-state relaxation. Nat. Methods **4**, 81–86 (2007). DOI: https://doi.org/10.1038/nmeth986
19. Kazemipour, A., et al. Kilohertz frame-rate two-photon tomography. Preprint at https://www.biorxiv.org/content/early/2018/06/28/357269 (2018).
20. Tsyboulski, D., Orlova, N., Ledochowitsch, P. & Saggau P. Two-photon frequency division multiplexing for functional *in vivo* imaging: a feasibility study. Preprint at https://www.biorxiv.org/content/early/2018/08/31/405118 (2018).
21. Chauhan, V., Bowlan, P., Cohen, J. & Trebino R. Single-diffraction-grating and prism pulse compressors. App. Optics **4**, 619–624 (2010). DOI: https://doi.org/10.1364/JOSAB.27.000619
22. Lu, R., et al. Video-rate volumetric functional imaging of the brain at synaptic resolution. Nat. Neurosci. **20**, 620–628 (2017). DOI: https://doi.org/10.1038/nn.4516
23. Wilt, B.A., Fitzgerald, J.E. & Schnitzer, M. J. Photon shot noise limits on optical detection of neuronal spikes and estimation of spike timing. Biophys. J. **104**, 51–62 (2013). DOI: https://doi.org/10.1016/j.bpj.2012.07.058
24. Wardill, T.J., *et al.* A neuron-based screening platform for optimizing genetically-encoded calcium indicators. PLoS One **8**, e77728 (2013). DOI: https://doi.org/10.1371/journal.pone.0077728
25. Madisen, L., *et al.* Transgenic mice for intersectional targeting of neural sensors and effectors with high specificity and performance. Neuron **85**, 942–958 (2015).

DOI: https://doi.org/10.1016/j.neuron.2015.02.022

26. Madisen, L., *et al.* A robust and high-throughput Cre reporting and characterization system for the whole mouse brain. Nat. Neurosci. **13**, 133–140 (2010). DOI: https://doi.org/10.1038/nn.2467

27. Schindelin, J., et al. Fiji: an open-source platform for biological-image analysis. Nat. Methods **9**, 676–682 (2012). DOI: https://doi.org/10.1038/nmeth.2019